Effects of boric acid on volatile tellurium in severe accident conditions

Annals of Nuclear Energy 200 (2024) 110412

Contents lists available at ScienceDirect

Annals of Nuclear Energy

journal homepage: www.elsevier.com/locate/anucene

Effects of boric acid on volatile tellurium in severe accident conditions

Fredrik Börjesson Sandén [a,*], Anna-Elina Pasi [b], Teemu Kärkelä [b], Tuula Kajolinna [b], Christian Ekberg [a]

[a] Chalmers University of Technology, Kemivägen 4, SE-412 96 Gothenburg, Sweden
[b] VTT Technical Research Centre of Finland Ltd, P.O. Box 1000, FI-02044 VTT, Espoo, Finland

ARTICLE INFO

Keywords:
Tellurium
Severe accidents
Boric acid
Fission product
XPS

ABSTRACT

Boric acid is used in light-water nuclear reactors to control the reactor and is expected to be present as part of the chemistry of a severe accident. Therefore, its influence on other prominent species expected in an accident must be investigated. One such species is tellurium. In the present study, tellurium is volatized, and boric acid is dissolved and injected into the system as a means of studying the interaction between it and tellurium. The experiments were evaluated with ICP-MS and XPS. Results suggest that while there is no direct interaction, boric acid still affects the tendency for tellurium to oxidize. In general, less oxidation was detected in the presence of boric acid than in its absence, especially at high temperatures. The species formed upon oxidation was determined to be TeO_2. Since tellurium metal is more volatile than TeO_2, this may have implication in a wider severe accident context.

1. Introduction

Nuclear energy, while being plannable and having negligible emissions of greenhouse gases (Sims et al., 2003), has proven to have certain disadvantages as well. Among the most visible disadvantages is the risk of severe accidents, such as Fukushima and Chernobyl. As such, for nuclear power to be a realistic choice for energy production, such accidents need to be studied and researched carefully to mitigate the consequences. Severe nuclear accidents differ from almost all other industrial accidents because of the presence of radioactive substances. Radiation carries the risk of acute radiation damage if the doses are high enough, but can also trigger carcinogenic diseases much later in life (Kazakov et al., 1992).

The radioactivity present in a nuclear power plant originates from the fuel and activation of structural materials. In the fuel, the radiation level is increased with fuel burnup due to the formation of highly radioactive fission products, such as iodine and cesium, both of which have been studied extensively both in larger experimental programs (March and Simondi-Teisseire, 2013; Clément and Zeyen, 2013) and smaller reports focusing on certain specific phenomena (Hou et al., 2013; Awual et al., 2014). Another notorious fission product is tellurium, which decays to form iodine. The decay means that the tellurium release will function as a delayed source of iodine with the potential to bypass countermeasures specifically targeted to iodine. Chemically, tellurium is highly variable and can occur in several different forms, including as organic species. Compared to iodine and cesium, it is significantly less studied.

A common choice for a neutron absorber in a nuclear reactor is boron, and control rods tend to incorporate this element. They were in use for instance in the Chernobyl plant and the Fukushima-Daiichi plant (boron carbide (Atomic Energy Society of Japan, 2014)). However, the most common reactor type, the pressurized water reactor (PWR), also makes use of dissolved orthoboric acid (henceforth referred to as just "boric acid"), both for regular operation and as an emergency system (Neeb, 1997). This means that boric acid or products derived from it most likely will be present in several chemical forms during an accident scenario. Tellurium and boron are known to interact with each other in certain situations. The oxides TeO_2 and B_2O_3, both of which can potentially form in a nuclear accident, are for instance known to form glasses (Bürger et al., 1984), though the temperature of this reaction exceeds the expected temperatures in the nuclear containment. Nevertheless, formation of similar species would be expected to strongly affect the tellurium behavior, especially the volatility. The aim of this paper is to determine whether tellurium and boron interact in nuclear accident-like conditions and investigate if and how the volatility of tellurium changes due to the presence of boric acid.

* Corresponding author.
E-mail address: sandenf@chalmers.se (F. Börjesson Sandén).

https://doi.org/10.1016/j.anucene.2024.110412
Received 14 December 2023; Received in revised form 26 January 2024; Accepted 5 February 2024
Available online 10 February 2024

2. Theory and background

2.1. Tellurium

Nuclear accidents present complex and variable chemical environments depending on, for example, the reactor type and the accident nature. Temperatures can vary from thousands of degrees inside the reactor core to near ambient temperatures outside of the containment, and atmospheric condition can likewise be oxidizing or reducing due to the reaction between zircalloy and water, with varying levels of steam present.

In total, dozens of tellurium nuclides are known to exist. However, significantly fewer makes for a realistic hazard in an accident scenario, namely those with a long enough half-life to pose a risk to the public after release. For radiation protection purposes, the most relevant tellurium nuclides are ^{129m}Te with a half-life of 33.6 days and ^{132}Te with a half-life of 3.17 days (Magill et al., 2015). Their respective releases during the Fukushima accident was 15 PBq and 180 PBq (Steinhauser et al., 2014).

Tellurium is a chemically complex element which melts at 449.5 °C and boils at 988 °C. It exists in five principal oxidation states (−2, 0, +2, +4 and +6). It belongs to the chalcogen group, same as oxygen. When heated in the presence of oxygen, tellurium forms tellurium dioxide TeO_2. It has a higher melting and boiling point, at 732 °C and 1245 °C respectively, though its volatility can be increased in the presence of steam, possibly due to the formation of $TeO(OH_2)$ (Medina-Cruz et al., 2020). TeO_2 is an amphoteric compound, behaving as a base in acidic media, and as an acid in alkaline media. Its solubility in water is poor. If oxidized further, for instance with hydrogen peroxide, it forms telluric acid $Te(OH)_6$ (Medina-Cruz et al., 2020).

Just like the lighter chalcogens, tellurium can react with hydrogen and form an analogue of water, named hydrogen telluride, H_2Te. It is a colorless gas with a pungent odor which decomposes quickly in air at temperatures below 627 °C. (Garisto, 1992; Medina-Cruz et al., 2020). The thermodynamics of the formation has been reported by Edward (1987). The formation can be expressed as seen in Reaction 1.

$$\frac{1}{2}Te_2(g) + H_2(g) \rightleftharpoons H_2Te(g) \qquad \text{(Reaction 1)}$$

The corresponding equilibrium constant for this reaction is given by Equation 1, where K is the equilibrium constant, and P indicates the different partial pressures. From this reaction, an increase in the H_2/Te ratio (a high partial pressure of hydrogen) pushes the reaction to the right (Garisto, 1992).

$$K = \frac{P_{H_2Te}}{\sqrt{P_{Te_2}} \times P_{H_2}} \qquad (1)$$

Due to the square-root in the denominator, a change in the tellurium partial pressure has a relatively low bearing on the hydrogen telluride. As the tellurium partial pressure decreases, thermodynamically, a proportionally larger part of the tellurium can be expected to appear as H_2Te (Garisto, 1992), though K itself never changes. However, hydrogen telluride decomposes quickly in moisture to form elemental tellurium.

Tellurium can also corrode steel under certain circumstances. If 316 l stainless steel is submerged in molten tellurium at 551 °C, it will corrode the steel and form a scale of metal tellurides on the form MTe_2, where M can be Fe, Cr or Ni. This is a fast process, as Martinelli et al. dissolved a 10x30x0.5 mm steel sample completely in 10 min (Martinelli et al., 2019). The reaction was a direct interaction and dissolution of the alloying elements iron, chromium, and nickel with tellurium (Pulham and Richards, 1990).

2.2. Boron from a nuclear perspective

Boron is present in nuclear installations due to its excellent neutron absorbing properties. In order to safely operate a nuclear reactor, the neutron economy must be carefully maintained. Control rods are used to increase or decrease the reactivity of the core as is needed, and function by being made from a neutron absorbing material. There are several designs where boron-based materials such as boron carbide or boron nitrate are used.

Aside from the control rods, boron has another application PWR: s. In this design, the water in direct contact with the reactor is isolated, meaning that additions to the water directly can be used to change the moderating properties of the water by addition of boron (Connolly, 1978). Typically, the control rods are used to change the neutron flux in the reactor in the short term, while varying the boric acid concentration is used to compensate for long-term changes in the fuel reactivity (Wiesman, 1977). This means that accidents in PWR systems may well include boric acid, or its derivatives, as part of the accident chemistry. Concentrations of boric acid in the primary circuit depends on the freshness of the fuel in the reactor, where fresh fuel necessitates a higher boron concentration. At first startup, when the entire core is using fresh fuel, the concentration can be as high as 2 g/l boron (of natural isomeric composition), and about 1 g/l at the beginning of a normal fuel cycle down to just a few mg at the end of the cycle (Neeb, 1997). In the case of an emergency, a concentrated solution of 2200 ppm of boron is injected (Neeb, 1997).

Boric acid undergoes sequential dehydration as it is heated. The reactions and relevant temperatures are given in the Reactions 2, 3 and 4 (Kaur et al., 2021).

$$B(OH)_3 \rightleftharpoons HBO_2 + H_2O,\ T\ 142^oC \qquad \text{(Reaction 2)}$$

$$4HBO_2 \rightleftharpoons H_2B_4O_7 + H_2O,\ T\ 167^oC \qquad \text{(Reaction 3)}$$

$$H_2B_4O_7 \rightleftharpoons 2B_2O_3 + H_2O,\ T\ 327^oC \qquad \text{(Reaction 4)}$$

$B(OH)_3$ melts 169 °C (Huo et al., 2019), and B_2O_3 at 500 °C (Hildenbrand et al., 1963).

However, thermodynamic calculations seem to indicate that transport of these compounds mainly occurs as boric acid or the trimer of metaboric acid ($H_3B_3O_6$) in temperatures between 180 °C and 727 °C. (Gouëllo et al., 2021). In a nuclear accident scenario, boric acid has previously been shown to be a factor that should be accounted for. In the case of the volatile fission products cesium and iodine, they often appear together as CsI aerosols. Their reaction will depend on the accident scenario, but in the presence of boric acid they can react to form cesium borates and gaseous iodine, according to the Reactions 5 and 6 (Gouëllo et al., 2021).

$$CsI(c) + B(OH)_3(g) \rightleftharpoons CsBO_2(c) + HI(g) + H_2O \qquad \text{(Reaction 5)}$$

$$2HI(g) \rightleftharpoons I_2(g) + 2H_2(g) \qquad \text{(Reaction 6)}$$

Tellurium is chemically different from both iodine and cesium, and its interaction with boric acid is unknown. The purpose of this paper is to investigate the effect of boric acid upon tellurium aerosols in conditions like those in a severe accident. This will be followed by a second paper to study the interactions in the same system, while also including iodine and cesium.

3. Method

A total of twelve experiments were conducted, and the experimental conditions are described in Table 1. Three atmospheric conditions (oxidizing, inert and reducing) were investigated and two temperatures, 300 °C and 650 °C were chosen, as similar temperatures have been used to simulate the primary circuit during a severe accident before (Clément and Zeyen, 2013). Boric acid undergoes its final dehydration at about 330 °C. Thus, with these two temperatures, the boric acid speciation may be different between the two conditions. Finally, boric acid and

Table 1
Experimental matrix for the study of interactions between tellurium and boric acid.

Experiment designation	Temperature [°C]	Atmosphere	Injection
Ref_Ox_LT	300	Oxidizing (Air)	–
Exp_Ox_LT	300	Oxidizing (Air)	$B(OH)_3$ (aq)
Ref_Ox_HT	650	Oxidizing (Air)	–
Exp_Ox_HT	650	Oxidizing (Air)	$B(OH)_3$ (aq)
Ref_In_LT	300	Inert (N_2)	–
Exp_In_LT	300	Inert (N_2)	$B(OH)_3$ (aq)
Ref_In_HT	650	Inert (N_2)	–
Exp_In_HT	650	Inert (N_2)	$B(OH)_3$ (aq)
Ref_Rd_LT	300	Reducing (H_2/Ar)	–
Exp_Rd_LT	300	Reducing (H_2/Ar)	$B(OH)_3$ (aq)
Ref_Rd_HT	650	Reducing (H_2/Ar)	–
Exp_Rd_HT	650	Reducing (H_2/Ar)	$B(OH)_3$ (aq)

water are injected into the carrier gas for all three atmospheric conditions.

Throughout all of these experiments, only singlets were performed, meaning that uncertainty analysis based on repeated experiments is not possible.

3.1. Experimental setup

The system used is one that has been used before to study the volatility of tellurium (Pasi et al., 2023), housed at VTT, Espoo in Finland. It is described in Fig. 1.

Both the reaction furnaces (tubular flow furnaces, Entech Vecstar, VCTF 4) used tubes made of stainless steel (AiSI 316l) to carry out the experiments. The volatilization furnace was set to 540 °C, and the reaction furnace was set to either 300 °C or 650 °C, depending on the experiment. The volatilization furnace was loaded with a total of 5 g tellurium metal powder (Te, Sigma-Aldrich, purity ≥99.997 %), placed in an alumina "boat" crucible in the middle of the heating section. With the slightly higher volatilization temperature compared to the melting point of tellurium, volatilization was relatively even across the experiments. With the high amount of tellurium, several experiments could be run in sequence without the need for the furnaces to cool down, meaning the conditions between most experiments using the same atmosphere could be kept relatively constant.

The experiments in inert and reducing atmosphere were ran in the following order: first the low-temperature reference experiment, followed by the low-temperature experiment with boric acid, followed by the high-temperature reference experiment, and finally the high-temperature acid experiment. Between each experiment, the filters (MilliPore, MitexTM PTFE, pore size 5 μm) and the liquid trap (0.1 M NaOH) were changed. For the oxidizing conditions it was feared that such a process would oxidize all of the precursor (the oxidation reaction is fast enough at 540 °C to affect the release of the tellurium precursor) towards the latter experiments, and so the four oxidizing conditions were conducted in two stages, with the two low-temperature experiments being run in sequence, where after the precursor was changed. The corresponding high-temperature experiments were run in sequence after. Following the experiment completion and the cooldown of the furnaces, the system was washed, and the precursor was retrieved. The mass of the precursor after the experiment was never below 3 g.

In principle the process of forming hydrogen telluride as described in reaction 1, could happen in the volatilization furnace and decrease the availability of tellurium in the latter experiments ran in the reducing atmosphere. However, as hydrogen telluride is unstable at the volatilization temperature, such an interaction is not expected to have any effect on the results.

The total gas flow through the reaction furnace was 6 l/min, supplied from two places; 3 l/min were fed through the volatilization furnace, and 3 l/min were added through the middle junction, alongside the boric acid for the experiments that used it. The gas flows were regulated through mass-flow control units (Brooks S5851, Brooks® Instrument). The water or the boric acid solution was fed through an atomizer (TSI model 3076). The boric acid concentration was 0.2 M.

Following the reaction furnace, 5 l/min of the gas stream was directed through the filter to collect any aerosol particles, and then proceeded through a liquid trap to catch any gaseous species. The final 1 l/min of the gas flow was diverted prior to the filter sampling. This gas was diluted and quenched with 10 l/min N_2 gas and then fed through the online measurement devices FTIR (fourier-transformed infrared spectroscopy), ELPI (electric low-pressure impactor), TEOM (tapered element oscillating microbalance, Rupprecht Patashnick Co., Inc. series 1400A).

Before the experiments began, the system was continuously flushed with N_2 until the setpoint of both furnaces were reached, and each experimental condition lasted for 30 min. After that time had passed, the gas flow was diverted to an exhaust while the filters and liquid traps were changed. After concluding an experiment series, the precursor was also collected for analysis with powder x-ray diffraction (PXRD).

The filters were weighed with a bench scale (Mettler Toledo XPE204) to the precision of one tenth of a milligram before and after the experiment to determine the weight of the collected material. After the filter's

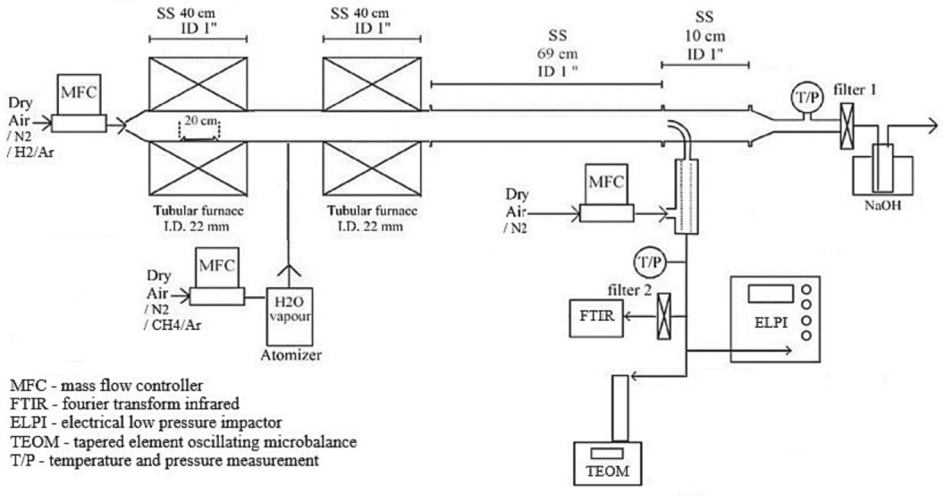

Fig. 1. Schematic depiction of the experimental setup used for the study.

retrieval, it was kept in a petri dish wrapped in parafilm and stored at room temperature. The filters were analyzed with XPS (X-ray photoelectron spectroscopy), within one week.

A mass balance could not be established due to significant deposition of tellurium at the junction between the furnaces, as well as in the tubing after the reaction furnace. Heating bands were used, but proved insufficient to prevent the deposition, especially at the junction where boric acid solution was added.

3.2. Analytical methods

3.2.1. ICP-MS

The elemental content of the liquid traps was measured with High resolution ICP-MS (inductively coupled plasma mass spectroscopy, Element 2, ThermoScientific) to determine the amount and species of the elements capable of penetrating the filters. The detection limit for tellurium (Te^{126}) was 0.006 ppb. The samples were diluted with 0.5 M HNO_3 (Suprapure) for the measurements.

3.2.2. XPS

The XPS machine used to analyze the filters was a PHI5000 VersaProbe III- Scanning XPS Microprobe™, using a monochromatic AlKα x-ray source (1486 eV). The beam width was 100 μm, 25 W 15 kV. FWHM was 0.654 eV. The system was aligned with Au (83.96 eV), Ag (368.21 eV) and Cu (932.62 eV), and the narrow scan measurements were aligned with the C1s signal at 284.6 eV before analysis.

Survey scan proceeded from 0 to 1100 eV with a step size of 1 eV, and the narrow scans proceeded over the selected region for the relevant element, with a step-size of 0.1 eV. For the C1s signal the step size was 0.05 eV.

3.2.3. PXRD

The precursors were analyzed in PXRD. The instrument was Bruker D8 Discover with a Cu Kα x-ray source. Measurement began at 20° and ended at 80°. The current and voltage in the X-ray source was 40 mA and 40 kV, respectively. Analysis was performed with the DIFFRAC.EVA software, version 5.2.

3.3. XPS binding energies and sensitivity factors

XPS (X-ray photoelectron spectroscopy) is a surface sensitive method of analysis that can be used to identify elements and their relative abundance in a sample. Furthermore, the chemical state of the elements in the sample can also be determined by XPS, through shifts in the measured binding energy. Table 2 lists several species relevant for tellurium and boron, and the binding energies associated with them (NIST X-ray Photoelectron Spectroscopy Database, 2012). The tellurium chemical state was investigated based on the $3d_{5/2}$-signal, and the oxygen and boron were both investigated based on their respective 1S signal.

Elemental compositions of the examined surfaces can be calculated according to Eq. (2)

$$C_x = \frac{\frac{I_x}{S_x}}{\sum_i \frac{I_i}{S_i}} \quad (2)$$

Where "I" is the measured peak area, "S" is the designated peak sensitivity factor, subscript "x" is the species of interest, subscript "i" is every species in the sample, and C is the calculated amount of element x in the sample surface (Stevie and Donley, 2020). The sensitivity factors account for the fact that different signals are easier to measure than others, with a high sensitivity factor for a signal indicating it is easily measured. This also means that a very clear signal does not necessarily mean a high concentration of that element in the sample. The calculation of the surface composition is based on the specific signals and sensitivity factors listed in Table 3.

The sensitivity factors used are supplied by the software used for the analysis; MultiPak Version 9.7.0.1, Ulvac-phi inc. Note that the analysis of the chemical state for tellurium is based on the $3d_{5/2}$- signal, and the abundance calculation uses the 4d-signal.

Table 2
Binding energies for various compounds as measured by XPS (NIST X-ray Photoelectron Spectroscopy Database, 2012). There is no reported energy level for the oxygen of TeO_3 or $Te(OH)_6$.

Compound	Binding energy (Te-$3d_{5/2}$) [eV]	Binding energy (B- 1S) [eV]	Binding energy (O-1S) [eV]
Te	572.9–573.54	–	–
TeO_2	575.6 eV- 576.5	–	530.1–530.7
TeO_3	576.6–577.3	–	–
TeO_3*$3H_2O$ (or $Te(OH)_6$)	577.1	–	–
B	–	186.5–188.5	–
$B(OH)_3$	–	192.8–193.6	533.4
B_2O_3	–	192.0–193.7	532.5–533.8

4. Results and discussion.

4.1. Filter weights

The filters were weighted with a bench scale with the precision of one tenth milligram before and after the experiment. The mass accumulated on the filters during the experiments can be seen in Fig. 2.

Two things are clear: there is a decreasing trend as the experiment progresses, and the reducing conditions consistently give the highest mass of aerosol particles on the filters. The decreasing trend can be explained by small leaks in the system, admitting some oxygen even in the case of inert and reducing conditions. This was seen on the precursor after the experiments and affected the inert systems more than the reducing one, presumably as the oxygen reacted to form water in the latter case. This then explains the higher filter mass for the early experiments, as the oxidation of the precursor increased gradually. For the oxidizing conditions a similar logic applies. Since those experiments were performed in two parts with fresh precursor for the high- and low-temperature experiments, the high masses in both the oxidizing reference cases can be justified; since those experiments used fresh precursor, some unoxidized tellurium reaches the filter and contributes to the weight. After some time in the oxidizing conditions, when the experiment with the acid begins, the precursor is largely oxidized already in the crucible and very little material can volatize and reach the filter.

As only singlets are performed, and due to progressive decrease in the filter mass accumulation, it is not possible from this result alone to certainly state that transportation of tellurium aerosols increase due to the addition of boric acid. However, it is worth pointing out that the high-temperature experiment with boric acid added does show a small increase in filter mass for both the inert and reducing conditions, even though the precursor should become less and less accessible as the experiment progresses. It seems like the acid solution may induce a slight increase in tellurium volatility. This idea is reinforced by the XPS measurements, which indicates that oxidation happens to a lower degree in the systems involving the acid solution (see further chapter 4.5.). As oxidation decreases volatility in tellurium, these two results are

Table 3
Signals and their associated sensitivity factors used to calculate the relative compositions of the investigated surfaces.

Element	Signal	Sensitivity factor
Te	4d	1.721
B	1 s	0.171
O	1 s	0.733
C	1 s	0.314

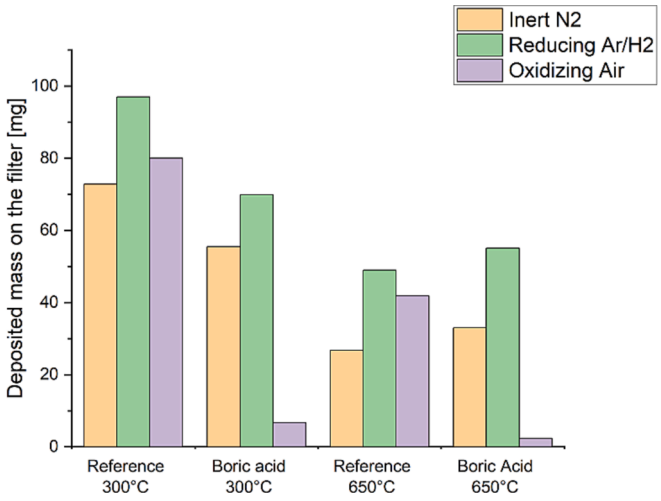

Fig. 2. Total material accumulated on each main-line filter after the respective experiment.

congruent.

4.2. Contents of the liquid traps

The contents of the liquid traps for the experiments can be found in Table 4. In general, the tellurium content of the liquid traps was very low except for in the high-temperature experiments in the reducing conditions. Boric acid, on the other hand, seems more likely to appear as a gaseous species at elevated temperatures, as the boron content is increased at the higher temperature.

ICP-MS does not allow for determination of chemical species, so it cannot be used to prove or disprove the presence of a Te-B species. However, if such a species forms, it should reasonably cause a change in the tellurium concentration compared to the corresponding reference case. In Table 4, this is seen twice, for the reducing and inert systems at high temperature.

For the high temperature experiments in the reducing atmosphere, the increase in tellurium content can possibly be explained by the formation of hydrogen telluride (H_2Te) in the reference case. The temperature of 650 °C is just high enough to enable its formation. If hydrogen telluride is formed in the high temperature reducing reference experiment, then it could also explain the decrease in tellurium content at the experiment involving boric acid. Since the acid was introduced dissolved in water, and hydrogen telluride decomposes in moist atmospheres, the reduction of tellurium content in the liquid trap in this case could be explained.

The high temperature experiment in inert atmosphere also display slightly more tellurium than the reference case, indicating that a Te-B could potentially be formed in this case. However, there is no indication of this when performing the XPS analysis, see further section 4.5. There is also no mention of any such species in the literature in similar conditions.

The contents of boron are slightly skewed by its presence in the glassware used for the liquid trap which explains the boron content in the reference cases. However, all experiments involving boric acid display heightened concentrations of boron, compared to the respective reference case. This applies for both high and low temperatures, though the increase is significantly higher at 650 °C.

Both the inert and the oxidizing atmosphere show comparatively high content of boron, indicating that boron can be transported as a volatile compound, or as a tiny aerosol (see further details in section 4.3-Online Analysis of Particles). At these temperatures, $B(OH)_3$ is expected to dehydrate quickly into B_2O_3, which has a negligible vapor pressure even at temperatures much higher than 650 °C (Cole and Taylor, 1935), implying transport as aerosols. The comparatively low boron content in reducing conditions implies that boron is less volatile in such an atmosphere. This may be tied to the large variance in particle diameter in reducing conditions (see section 4.3, and section 5.) though this assumption is not congruent with what is seen in from the XPS measurements (section 4.5), as no significant increase in boron content on the filter is detected at reducing conditions.

Table 4
Tellurium and boron contents of the liquid traps for the different experiments. Notice the different units for tellurium and boron.

Experiment Designation	Tellurium content [μmol/dm^3 trap solution]	Boron Content [mmol/ dm^3 trap solution]
Ref_In_LT	2.35	0.17
Exp_In_LT	2.35	1.57
Ref_In_HT	0	0.24
Exp_In_HT	0.78	6.15
Ref_Rd_LT	0.78	0.59
Exp_Rd_LT	0.78	0.75
Ref_Rd_HT	41.5	1.11
Exp_Rd_HT	7.05	3.27
Ref_Ox_LT	0.78	0.13
Exp_Ox_LT	0.78	2.16
Ref_Ox_HT	0.78	0.23
Exp_Ox_HT	0.78	10.37

4.3. Online analysis of particles

The properties of aerosols were online analyzed using ELPI and TEOM devices. The above given results for the accumulated mass of particles on filter were supported by the devices. Further details were extracted from the ELPI data to estimate the development of particle size in the experiments, see Fig. 3.

In general, the highest particle count median diameter (CMD) values were for the inert condition, except at high temperature reference condition in which reducing conditions resulted in the largest particle diameter. The CMD values decreased from inert to reducing conditions and from reducing to oxidizing conditions. It was expected the particle diameter to be low due to the low release of tellurium in an air

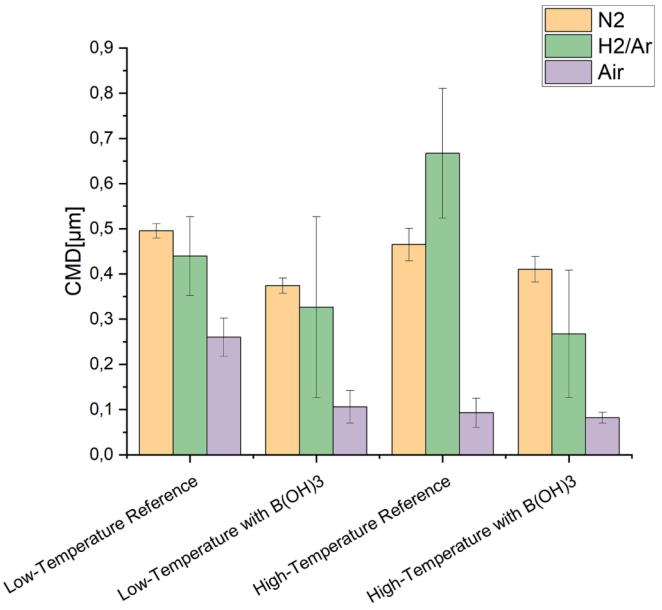

Fig. 3. Particle count median diameter (CMD) in the experiments. The average CMD with the actual minimum and maximum CMD values are given.

atmosphere (tellurium oxidation in the crucible decreases the release). The span of particle diameters was relatively low for both oxidizing and inert conditions, but much bigger for the reducing case.

4.4. FTIR analysis of gaseous species

The properties of gas phase species were online analyzed using FTIR device. In general, the analysis results were showing the expected fed component H_2O with some trace level CO_2 and CO from the laboratory air. The water content ranged ca. from 0.9 to 1.3 vol-% in the experiments and water was observed when boric acid solution was fed using atomizer.

4.5. XPS analysis of the filters

The results for the XPS consists of, for each sample, a survey scan to determine the elemental composition and abundance, as well as a more detailed scan over a small energy range in order to determine the chemical environment of each element. The following section will only present a selection of representative or important spectra. In most cases the survey spectrum looks nearly identical between the samples, differing only in the relative intensities between the peaks. An example of such a spectrum is seen in Fig. 4.

The XPS spectrum for the reference cases in inert and reducing conditions look similar for both the high and low temperature experiments. The spectra for the low-temperature experiment for the inert and the reducing conditions are presented in Fig. 5.

All systems exhibit the same tellurium speciation; one signal is in the area 573.01 eV- 573.12 eV, and another at 576.32 eV- 576.48 eV. Furthermore, the distribution of metallic tellurium and Te(IV) between the systems, and the element composition of the systems both remain almost constant, as can be seen in Table 5. The lower energy signal matches the reported measurements for pure tellurium metal reasonably well. The second signal matches the values reported for TeO_2. Both of these compounds are also reasonable considering the systems; metallic tellurium is the dominant species, with some contamination from oxygen, forming TeO_2.

The appearance of Te(IV) in both the reducing and inert conditions is considered the "baseline" content of Te(IV) for the filters. Most likely this comes from trace amounts of oxygen left in the system during the experiments, or from the time the filters are exposed to the open air in between the experiment and the XPS measurement. The filters retrieved from the inert atmosphere were measured in the XPS only after 7 days, whereas the experiments conducted in reducing atmosphere were measured after 4 days. As can be seen in Table 5, the samples from the reducing atmosphere had a slightly higher ratio of Tellurium metal to Tellurium oxide. However, the relative amount of TeO_2 and tellurium metal were rather similar across all reference cases.

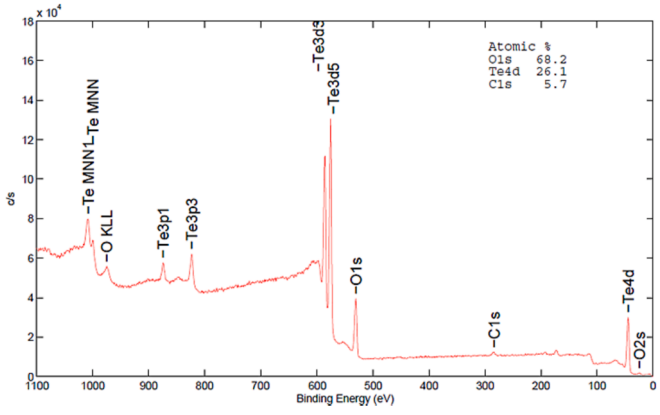

Fig. 4. Survey spectrum of the High-temperature reference spectrum in air atmosphere. The sample predictably contains tellurium, oxygen, and a small contamination of carbon, most likely dust from the sample transport.

The oxygen content is comparatively high relative to the ratio of metallic to oxidized tellurium. However, considering the system with only tellurium and a reducing or inert carrier gas, and the binding energies of the XPS measurements, no other species than TeO_2 can reliably explain the Te(IV) oxidation state. The high-temperature references especially give slightly conflicting results in that the survey measurement imply a large oxidation, whereas the detailed scan of the 3d 5/2 signal instead indicates mostly metallic tellurium.

The oxidizing system behaved differently. The spectrum for both the high- and the low-temperature conditions are displayed in Fig. 6.

As could be expected, the amount of unoxidized metal is very low or completely absent in this system. The + IV oxidation state dominates the high-temperature system completely, whereas the low-temperature system consists of roughly equal parts of a compound with the binding energy 576.17 eV, presumably TeO_2, and a compound with the binding energy 578.03 eV. This energy is higher than any tellurium-oxygen species listed in the database. It is presumed to indicate TeO_3. Since the trioxide is less stable than the dioxide, this assumption explains why the + VI state is not seen in the high-temperature reference.

4.5.1. XPS results- added boric acid solution

The survey spectra again look almost the same for all cases, both high and low temperature experiment, with the one difference being the boron content of the filters. The measured boron contents for the respective samples can be found in Table 6. A comparison of two surveying spectra can be seen in Fig. 7.

For the three low-temperature experiments conducted in the presence of boric acid solution, the XPS measurement of the inert and reducing systems all look very similar to their respective reference cases, as seen in Fig. 8. There is nothing in any of the tellurium spectra that indicates a new species, though there are signals for boron, as well as a change in the oxygen spectrum, matching the oxygen signal for boric acid or B_2O_3 (NIST X-ray Photoelectron Spectroscopy Database, 2012).

While no new tellurium species form, the ratio of metallic to oxidized tellurium has changed due to the addition of boric acid solution, as can be seen in Table 6. While not a large change, the ratio has shifted towards less oxidation compared to the reference cases.

For the high temperature experiments, there is again no indication that tellurium has interacted directly with the boric acid, or any products formed from it. Again, the tellurium spectra are similar to their reference cases for their respective atmosphere.

Furthermore, the degree of oxidation on the sample has changed significantly compared to the reference cases. The oxidizing condition results in complete oxidization of the tellurium to TeO_2, which is not unexpected. However, the low amount of oxidation on the samples from the reducing and inert conditions compared to the references seems to indicate that the oxidation process is inhibited to some degree. See also Table 6. Both in high- and low- temperature conditions all the cases where acid solution is included display significantly lower amounts of Te (IV), indicating that the presence of boric acid serves to further reduce the metal or, more likely, preventing its oxidation.

This may have to do with the pattern seen in Table 4. The increase in tellurium content in the liquid traps following the boric acid experiments may be due to decreased oxidation in those cases. The high temperature reducing condition is the only system where this increase was not seen, but in this case the tellurium can already form a volatile compound in H_2Te.

The oxidizing cases both for high-and low temperature conditions display significant contents of boron, something which is not seen for reducing or inert conditions. Studying the respective high-resolution spectrum places the boron binding energy at 192.9–193.5 eV for every case but one. The low-temperature experiment with boric acid in air has the boron signal also at 195.4. This spectrum is shown in Fig. 9 the 193-signal is assumed to belong to boric acid or B_2O_3. These are difficult to

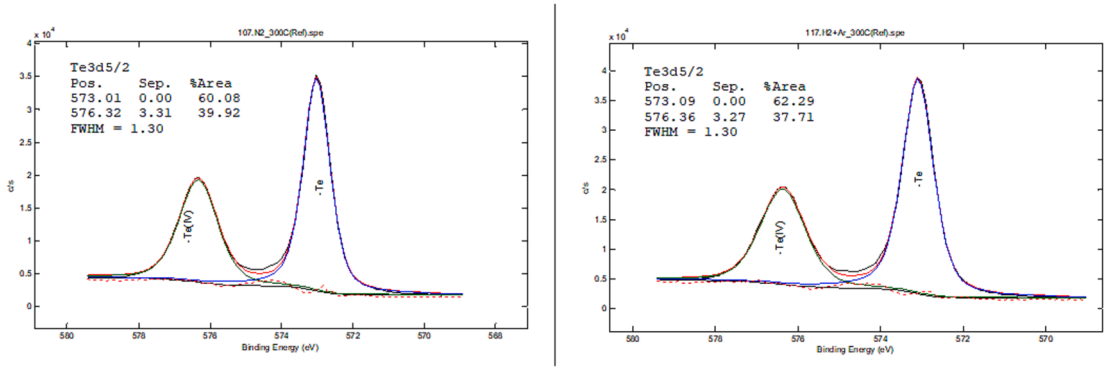

Fig. 5. The XPS spectra of the reference cases. The spectra on the left-hand side are for the inert system, and the right-hand side are for the reducing system, both at the temperature of 300 °C.

Table 5
Contents of the reference filters, and the ratio between Tellurium metal and TeO_2 in the references for reducing and inert atmosphere. Note that the contents do not add up to 100 %. This is due to some interference from the underlying PTFE-filter.

System	Te- content [%]	O- content [%]	Te/Te(IV) ratio in the $3d_{5/2}$ signal
Ref_In_LT	47.2	52.8	1.8
Ref_Rd_LT	54.8	45.2	1.9
Ref_Ox_LT	30.6	69.4	0.1
Ref_In_HT	37.2	62.8	1.6
Ref_Rd_HT	50.5	49.5	1.9
Ref_Ox_HT	27.7	72.3	0

differentiate in the XPS, as both the boron and the oxygen signals tend to overlap. As for the signal at 195.4 eV, it fits reasonably well with boron fluorides BF_4^-, which could, in theory be formed from the fluoride in the PTFE-filter.

4.5.2. Results of remeasurement

To further investigate the hypothesis that the boric acid protects against oxidation, the high-temperature samples from the reducing atmosphere (both the reference sample and the sample exposed to boric acid) were measured again with the XPS. This measurement took place 13 days after the initial measurement, and the samples were exposed to the air in the meantime. The surface composition of the measured filters is reported in Table 7.

It appears that the presence of the boron compound, whether it is boric acid or B_2O_3, does indeed prevent oxidation of tellurium in ambient conditions. Of course, the above result has only been confirmed for the filters treated in reducing conditions. This result may be linked to a study performed by Zhang et al., where 316l steel was submerged in boric acid solutions for seven days. The EDX imaging of those surfaces revealed comparatively little oxygen content, compared to non-borated solutions (Zhang et al., 2018).

5. Conclusions

The presence of boric acid does not seem to result in any compounds composed of tellurium and boron together at the studied low temperature conditions of 300 and 650 °C. However, the presence of boric acid does seem to influence the tellurium in that the oxidation behavior changes upon exposure to boric acid. The XPS measurements consistently showed less oxidation on the samples exposed to boric acid than the corresponding reference samples. For the high-temperature experiments, this is supported by the filter wights, as they increase for the high temperature cases with boric acid compared to without. The theory thus is that boric acid or, perhaps more likely, B_2O_3 is deposited on the

Table 6
Ratio between Tellurium metal and TeO_2 in the experiments including boric acid.

System	Te- content [%]	O- content [%]	B-content [%]	Te/Te(IV) ratio
Exp_In_LT	52.5	39.8	8.5	2.4
Exp_Rd_LT	47.2	46.0	6.8	2.2
Exp_Ox_LT	9.1	67.1	21.7	0.1
Exp_In_HT	54.5	41.8	3.7	3.5
Exp_Rd_HT	54.2	34.4	11.3	3.0
Exp_Ox_HT	5.2	69	25.8	0

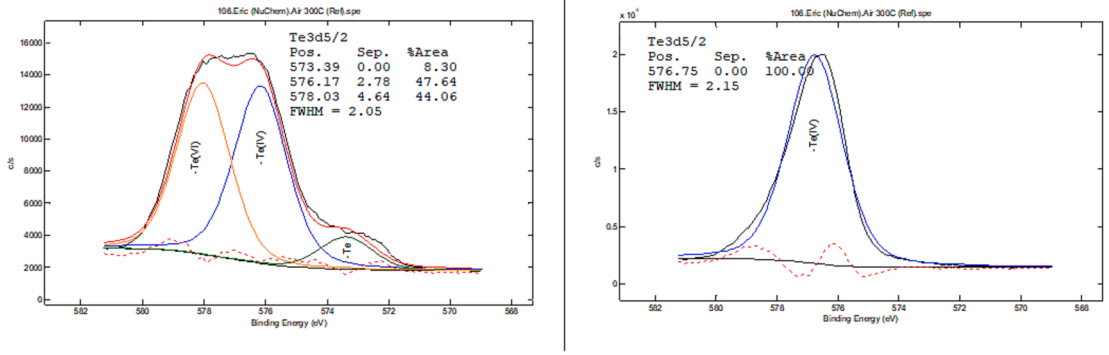

Fig. 6. The XPS spectra of the oxidizing reference cases. The spectrum on the left-hand side is for the system at 300 °C, and the right-hand side is for the system at 650 °C.

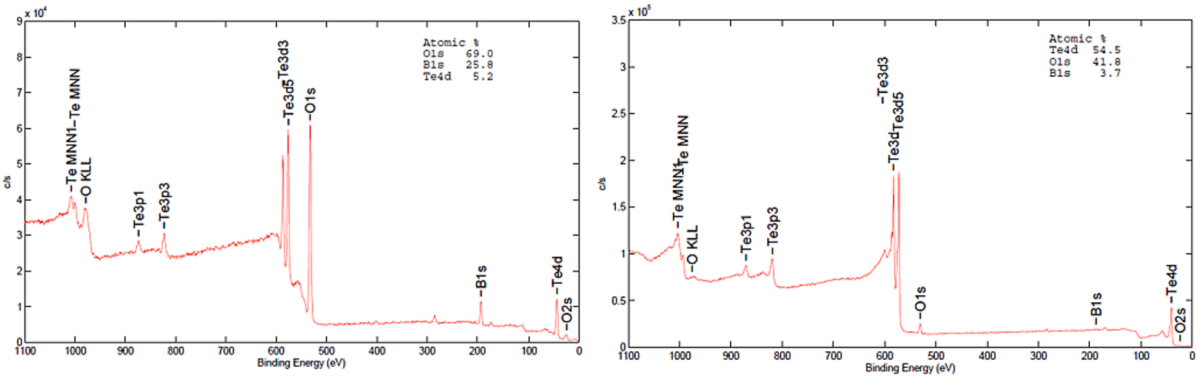

Fig. 7. Survey spectra of the experiments in high temperature involving boric acid. To the left, the experiment conducted in air, and to the right the experiment conducted under nitrogen atmosphere. Notice the different relative signal strength in the boron, at ca. 200 eV.

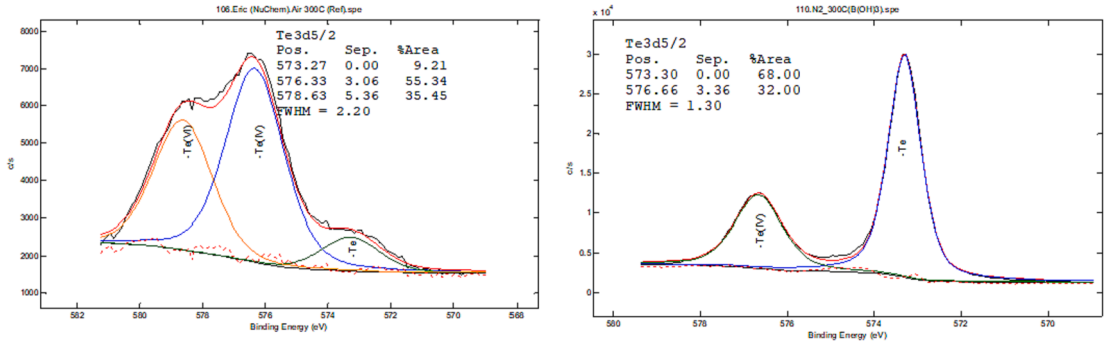

Fig. 8. XPS spectra for the experiments involving boric acid at 300 °C. To the right is the spectrum for inert conditions, which is nearly identical to the spectrum for reducing conditions. On the left is the spectrum for oxidizing conditions.

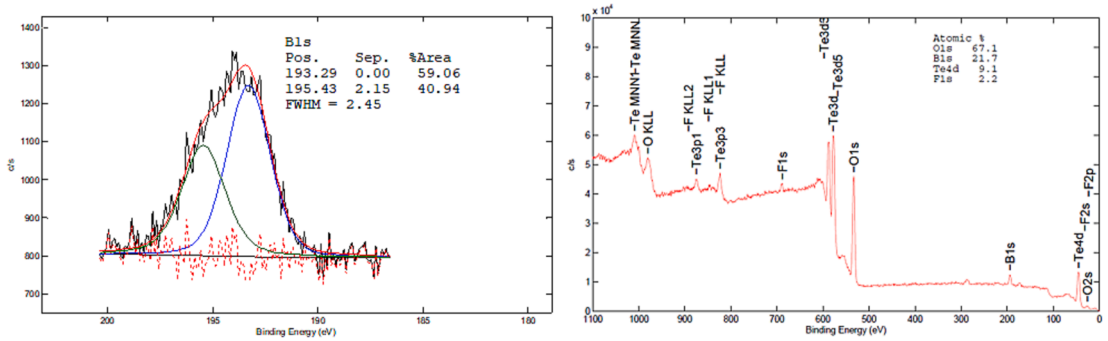

Fig. 9. High-resolution boron spectrum from the low temperature experiment in air atmosphere to the left. The signal is made up of two compounds, where one is either $B(OH)_3$ or B_2O_3. To the right is the corresponding survey spectrum, with the fluoride signal marked (around 700 eV).

Table 7
Change in filter surface composition for the filters exposed to high temperature and reducing conditions after 13 days of exposure to ambient conditions. The filter exposed to boric acid was almost unchanged.

Experiment	Initial measurement			Repeat measurement (Thirteen days later)		
	Te [%]	O [%]	B[%]	Te [%]	O [%]	B[%]
Ref_Rd_HT	50.5	49.5	–	29.1	70.9	–
Exp_Rd_HT	54.2	34.4	11.3	54.0	33.0	13.0

surface on the tellurium particles or alternatively on the filter and form a protective coating that prevents oxidation.

Tellurium is likely transported mainly as TeO_2 in oxidizing conditions, TeH_2 and tellurium aerosols in reducing conditions, and aerosols in inert conditions.

The transport of boron is less certain, as there is contamination from borosilicate glassware in the liquid trap, but there is indication that the transport of boron depends on the atmosphere and temperature. In the liquid trap, the boron content invariably increases for the high-temperature conditions, implying the formation of a compound capable of penetrating the filter. This increase is the largest in oxidizing conditions, though the effect is clearly seen in every condition.

The species responsible for the increase is presumed to be B_2O_3 as an aerosol. The dehydration reaction described in Reactions 2–4 are expected to be faster in the higher temperature, explaining the boron increase in the liquid trap in these cases. As for the increase in the oxidative atmosphere, it is assumed that a direct reaction between oxygen and boric acid complements the dehydration reaction. The overall reaction is presented in Reaction 7.

$$4\,B(OH)_3(g) + O_2(g) \leftrightharpoons 2B_2O_3(s) + 3\,H_2O\,(g) \qquad \text{(Reaction 7)}$$

The XPS-analysis of the filters also detects boron. For both inert and reducing conditions the contents are low, but the oxidizing conditions have significant amounts of boron in both temperatures. This then implies that boron may be transported as an aerosol in oxidizing conditions, though there is no indication in XPS of it being a Te-B-species. Again, it is presumed to be in the form of B_2O_3.

Under the investigated conditions, boron tends to appear in relatively high concentration in both in the liquid trap and on the filter in oxidizing conditions, or in modest amounts in both the trap and on the filter for reducing conditions. This implies that transport of boron happens as a tiny aerosol, somewhat capable of penetrating the filter. The ELPI measurements may also support this theory, as the oxidizing conditions measured the lowest mean particle diameter of all the conditions, implying smaller particles in this case.

CRediT authorship contribution statement

Fredrik Börjesson Sandén: . **Anna-Elina Pasi:** Writing – review & editing, Visualization, Software, Methodology, Formal analysis, Data curation, Conceptualization. **Teemu Kärkelä:** Writing – review & editing, Visualization, Supervision, Methodology, Investigation, Formal analysis, Data curation. **Tuula Kajolinna:** Formal analysis. **Christian Ekberg:** Writing – review & editing, Supervision, Funding acquisition.

Declaration of competing interest

The authors declare that they have no known competing financial interests or personal relationships that could have appeared to influence the work reported in this paper.

Data availability

Data will be made available on request.

Acknowledgements

This work was funded in part by the Nordic nuclear safety research organization (NKS) and APRI 11 (Accident Phenomena of Risk Importance, swedish nuclear safety research). Part of this work was performed at the Chalmers Material Analysis Laboratory, CMAL.

A special thanks to Eric Tam for assistance with the XPS analysis.

References

Atomic Energy Society of Japan, The Fukushima Daiichi Nuclear Accident-Final Report of the AESJ Investigation Committee, Maruzen Publishing Co., 2014, 508-514, 10.1007/978-4-431-55160-7, ISBN 978-4-431-55160-7, retrieved 2023-05-23.

Awual, M.R., Suzuki, S., Taguchi, T., Shiwaku, H., Okamoto, Y., Yaita, T., 2014. Radioactive cesium removal from nuclear wastewater by novel inorganic and conjugate absorbents. Chem. Eng. J. 242, 127–135. https://doi.org/10.1016/j.net.2021.10.026, retrieved 2023-09-13.

Beahm, E.C., 1987. Tellurium behavior in containment under light water reactor accident conditions. Nucl. Technol. 78 (3), 295–302. https://doi.org/10.13182/NT87-A15995, retrieved 2021-12-01.

Bürger, H., Vogel, W., Kozhukharov, V., Marinov, M., 1984. Phase equilibrium, glass-forming, properties and structure of glasses in the TeO_2-B_2O_3 system. J. Mater. Sci. 19, 403–412. https://doi.org/10.1007/BF00553563, retrieved 2023-05-16.

Clément, B., Zeyen, R., 2013. The objectives of the Phébus FP experimental programme and main findings. Ann. Nucl. Energy 61, 11–22. https://doi.org/10.1016/j.anucene.2013.03.037, retrieved 2021-11-29.

Cole, S.S., Taylor, N.W., 1935. The System Na2O-B2O3 IV Vapor pressures of boric oxide, sodium metaborate and and sodium diborate between 1150°C and 1400°C. J. Am. Ceram. Soc. 18, 82–85 retrieved 2023–12-01.

Connolly, T.J., 1978. Foundations of Nuclear Engineering. John Wiely & Sons Inc., pp. 207–282 retrieved 2023–09-13.

Garisto, F., 1992. Theromydnamic behaviour of Tellurium at high temperatures. INIS report nr: AECL—10691, retrieved 2023–05-30, Canada.

Gouëllo, M., Hokkinen, J., Suzuki, E., Horiguchi, N., Barrachin, M., Cousin, F., 2021. Interaction between caesium iodide particles and gaseous boric acid in a flowing system through a thermal gradient tube (1030 K–450 K) and analysis with ASTEC/SOPHAEROS. Prog. Nucl. Energy 138. https://doi.org/10.1016/j.pnucene.2021.103818, retrieved 2022-08-19.

Hildenbrand, D.L., Hall, W.F., Potter, N.D., 1963. Thermodynamics of vaporization of lithium oxide, boric oxide, and lithium metaborate. J. Chem. Phys. 39 (2), 296–301. https://doi.org/10.1063/1.1734245, retrieved 2023-11-03.

Hou, X., Povinec, P.P., Zhang, L., Shi, K., Biddulph, D., Chang, C., Fan, Y., Golser, R., Hou, Y., Ješkovský, M., Jull, A.J.T., Liu, Q., Luo, M., Steier, P., Zhou, W., 2013. Iodine-129 in seawater offshore Fukushima: distribution, inorganic speciation, sources, and budget. *Environ. Sci. Technol.* 47, 3091–3098. https://doi.org/10.1021/es304460k, retrieved 2023-09-13.

Huo, I., Zhu, Q., Li, S., Gao, J., Wang, Q., 2019. Effective assembly of a novel aluminum-oxynitride BaAl11O16N activated by Eu2+ and Mn2+ via salt-flux assistance and its photophysical investigation. J. Alloy. Compd. 787, 96–103. https://doi.org/10.1016/j.jallcom.2019.02.038, retrieved 2023-11-03.

Kaur, G., Kainth, S., Kumar, R., Sharma, P., Pandey, O.P., 2021. Reaction kinetics during non-isothermal solid-state synthesis of boron trioxide via boric acid dehydration. Reaction Kinet., Mech. Catal. 134, 347–359. https://doi.org/10.1007/s11144-021-02084-8, retrieved 2023-04-27.

Kazakov, V., Demidchik, E., Astakhova, L., 1992. Thyroid cancer after chernobyl. Nature 359, 21. https://doi.org/10.1038/359021a0, retrieved 2023-05-23.

Magill, J., Pfennig, G., Dreher, R., Sóti, Z., Nuklidkarte-, K., 2015. Chart of the Nuclides, 9th ed. Nucleonica GmbH. ISBN 978-3-943868-04-3.

March, P., Simondi-Teisseire, B., 2013. Overview of the facility and experiments performed in Phébus FP. Ann. Nucl. Energy 61, 11–22. https://doi.org/10.1016/j.anucene.2013.03.040, retrieved 2021-11-29.

Martinelli, L., Young, D.J., Gossé, S., Bosonnet, S., 2019. Corrosion of 316L in liquid tellurium at 551 °C. Corros. Sci. 151, 35–43. https://doi.org/10.1016/j.corsci.2019.02.001, retrieved 2023-05-31.

D. Medina-Cruz, W. Tien-Street, A. Vernet-Crua, B. Zhang, X. Huang, A. Murali, J. Chen, Y. Liu, J. Miguel Garcia-Martin, J. L. Cholula-Díaz, T. Webster, edited by : B. Li, T. Fintan Moriarty, T. Webster, M. Xing, Racing towards the Surface- Antimicrobial and Interface Tissue Engineering, Springer Nature Switzerland, 2020, ISBN 978-3-030-34470-2, https://doi.org/10.1007/978-3-030-34471-9, retrieved 2023-05-16.

Neeb, K.H., 1997. The Radiochemistry of Nuclear Power Plants With Light Water Reactors, Walter de Gruyter, 1997, pages 27-42, 477-495 retrieved 2021-08-11.

NIST X-ray Photoelectron Spectroscopy Database, NIST Standard Reference Database 20, version 4.1, last update to data content 2012, compiled by A.V. Naumkin, A. Kraut-Vass, S.W. Gaarenstroom, C.J. Powell, DOI:https://doi.org/10.18434/T4T88K, retrieved 2023-06-26.

Pasi, A.E., Kärkelä, T., Börjesson Sandén, F., Tapper, U., Kajolinna, T., Ekberg, C., 2023. Gas phase interactions between tellurium and organic material in severar nuclear accident scenarios. Ann. Nucl. Energy retrieved [2023-11-13].

Pulham, R.J., Richards, M.W., 1990. Chemical reactions of cesium, tellurium and oxygen with fast breeder reactor cladding alloys- part 1, the corrosion by tellurium. J. Nucl. Mater. 171, 319–326. https://doi.org/10.1016/0022-3115(90)90378-Z, retrieved 2023-09-12.

Sims, R.E.H., Rogner, H.H., Gregory, K., 2003. Carbon emission and mitigation cost comparison between fossil fuel and renewable energy resources for electricity generation. Energy Policy 31, 1315–1326. https://doi.org/10.1016/S0301-4215(02)00192-1, retrieved 17/5-2023.

Steinhauser, G., Brandl, A., Johnson, T.E., 2014. Comparison of the Chernobyl and Fukushima nuclear accidents: A review of the environmental impacts. Sci. Total Environ. 470–471, 800–817. https://doi.org/10.1016/j.scitotenv.2013.10.029 retrieved 2021-11-25.

Stevie, F.A., Donley, C.L., 2020. Introduction to X-ray photoelectron spectroscopy. J. Vac. Sci. Technol. A 38, 6. https://doi.org/10.1116/6.0000412, retrieved 2023-011-08.

Wiesman, J., 1977. Elements of Nuclear Reactor Design, Elsevier Scientific Publishing Company, Printed in Amsterdam, pages 1-47, retrieved 2023-09-13.

Zhang, S., Lu, Q., Xu, Y., He, K., Liang, K., Tan, Y., 2018. Corrosion behaviour of 316L stainless steel in boric acid solutions. retrieved 2023-11-30 Int. J. Electrochem. Sci. 13 (4), 3246–3256. https://doi.org/10.20964/2018.04.33,.